

Virtualization for the Purposes of Modeling and Computer Simulation of a Class of Overconstrained Robots

Nikolay Bratovanov
Robotics Lab, Faculty of Automation
Technical University of Sofia
Sofia, Bulgaria
nbratovanov@tu-sofia.bg

Zlatko Sotirov
Genmark Automation
Fremont, CA
zsotirov@genmarkautomation.com

Abstract—the paper presents an approach to modeling, analysis, and simulation of overconstrained parallel manipulators, based on joint virtualization. This novel concept is proposed for the purpose of studying a three-degree-of-freedom closed-loop mechanism, which has found a broad industrial application in the field of semiconductor device manufacturing and fab automation. A distinctive feature of this overconstrained manipulator, known as GPR, is its ability to “use” the inherent elasticity and backlash of its components in order to perform finite small rotations when in the vicinity of a singular configuration, eliminating the need of using additional kinematic joints. This characteristic behavior is exhaustively studied by introducing virtual joints at the GPR’s terminal link, allowing the development of precise computational models that facilitate the execution of realistic motion simulations (in 3D SolidWorks environment), as well as in-depth mobility and accuracy analyses, essential for the efficient implementation and optimization of the GPR in terms of both practice and theory.

Keywords—overconstrained mechanisms; parallel manipulators; kinematic modeling; computer simulations; joint virtualization; semiconductor industry automation; motion simulations; offline programming; SolidWorks API;

I. INTRODUCTION

Regardless of the already widespread industrial application of parallel robots (due to their numerous advantages over their serial counterparts [2], [4], [5], [7], [8]), the implementation of overconstrained parallel manipulators (OCPM) in industry is still quite limited [1], [3], [6]. In 1996, Genmark Automation, a corporation in California, developed and started to manufacture a special type of OCPM intended for the field of semiconductor device manufacturing and fab automation. The mechanism was named GPR and was trademarked and patented in 1996 [9]. It had three degrees of freedom (DOF) and was designed to perform two small independent rotations in the range of $\pm 1.5^\circ$, as well as one larger translation (up to 20"). Its terminal link (platform) was used as a basis for installing serial planar arms (one or two) with up to four DOF each. The resultant hybrid parallel-serial structure was capable of adapting to misaligned equipment and compensating for the deflection of the handled objects (wafers) [10] (Fig. 1). Since 1996, thousands of GPRs have been implemented in various fabs, turning out to be one of the largest industrial implementations of OCPM in the world.

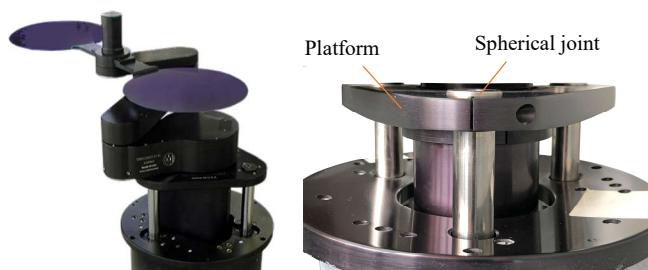


Figure 1. Substrate-handling robot (left) and structure of the GPR (right).

A distinctive feature of the GPR is the ability to “use” the inherent elasticity and backlash of its components in order to perform the required small rotations of the platform, instead of using additional kinematic joints. Such an original concept has many advantages, such as increased accuracy, reduced cost and simplified design. On the other hand, due to its overconstrained nature, the GPR has less mobility than required by the task. In other words, specific moves would not exist if the mechanism was ideal, becoming possible only because of its imperfections. Being quite specific, this behavior has not been adequately addressed in the literature and its study represents both research and practical interest. To precisely analyze and simulate the GPR’s mobility, its overconstrained structure has to be relieved by introducing virtual joints to the platform. It is important to remark that these joints are imaginary - they do not exist in the actual mechanism, and must be treated as a purely theoretical means, developed and used for GPR description purposes only. Previous paper of the same authors and co. proposes an initial approach for joint virtualization of the GPR [11]. This paper aims at extending the original work by developing even more realistic method, thus providing a more precise computational model. The last facilitates the performance of in-depth mobility and accuracy analyses, and allows the execution of efficient motion simulations in 3D environments – tasks with a great importance to the applicability and optimization of the GPR.

II. STRUCTURE AND FUNCTIONALITY OF THE GPR

The GPR is comprised of a base and a platform, connected together by three rods, which are parallel to each other. They are linked to the base via fifth-order sliding joints, whose axes are also parallel. The rods are connected to the platform via

spherical joints (Fig. 1). While the spherical joints are passive, the sliding joints are active, allowing the length of each rod with respect to the base flange to be individually controlled. The GPR's motion capabilities are highly beneficial for the process of handling silicon wafers/substrates between different locations (carriers, processing equipment, peripheral devices), where high reachability, superior precision, and tilting of the robot's end-effector are simultaneously required by the task.

III. NEED FOR VIRTUALIZATION OF THE GPR

In order to describe the mobility of the GPR, the concept of joint virtualization is proposed. It's a theoretical means, based on imaginary components (virtual joints), which add degrees of freedom to the GPR, thus "relieving" its overconstrained structure. The main purpose is to model the mechanism's inherent imperfections, reflect their contribution to the overall mobility and hence be able to solve its kinematics. In this way, complete mobility and accuracy analyses of the GPR become possible, which allow to quantitatively express the relationship between the components' elasticity/clearances and the amount of motion of the platform; to evaluate the undesirable effect of shifting the platform's center when tilting (as a result of the GPR's overconstrained nature); and to develop an exhaustive kinematic model that could be later used for the execution of precise motion simulations in a virtual 3D environment.

The essential need for performing motion simulations and offline programming of the GPR is one of the key factors that motivates the development of the present work. Currently, all substrate-handling manipulators, manufactured by Genmark Automation, are simulated in a 3D SolidWorks environment for application analysis, offline programming, and marketing purposes. This is done by using a custom tool for robot motion simulation and offline programming, based on SolidWorks API, that has been proposed and developed by the same author [12]. Despite its so far successful and efficient utilization, the recent versions of the tool were not capable of performing precise motion simulations and offline programming tasks, associated with GPR-based robots, simply because a complete description of the GPR's mobility was not available. To deal with this limitation, the following assumption was made – the platform was considered to perform two basic rotations about its X and Y axes, as if it wasn't attached to the three vertical rods at all. As a result of this simplification, the rods were forced out of the spherical bearing housings each time the platform was tilted (Fig. 2). More importantly, the actual shift of the center of the platform was not accounted for.

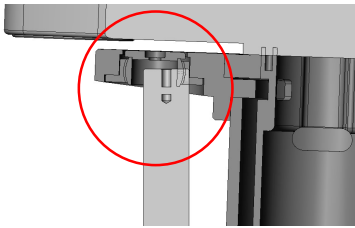


Figure 2. Platform tilting simulation, based on approximate GPR modeling.

Such inaccuracy, even though relatively small, could have a significant impact on the GPR offline programming procedure,

as well as on the overall effectiveness of the simulation tool in general, especially when dealing with absolute positioning robot applications. To solve this issue, a GPR virtualization approach, based on three radially-oriented sliding virtual joints has been proposed in the authors' previous work [11] (Fig. 3).

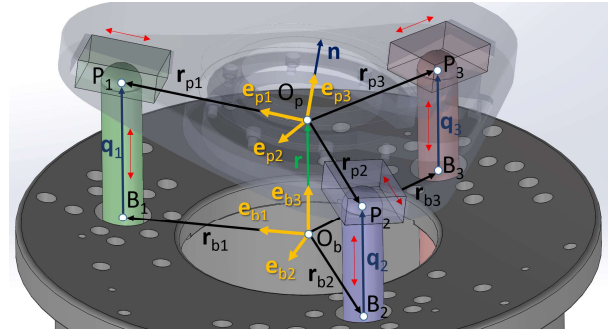


Figure 3. Geometry of the GPR and virtualization via three sliding joints.

In this manner, more precise modeling of the mechanism has been developed (once the forward and the inverse kinematics problems are solved) that allowed to establish the relationship between GPR's imperfections and the motion of the platform. In addition, the shifting of its center has also been investigated as a function of the tilting, making it possible to accommodate this model into the SolidWorks API-based motion simulation tool, and thus allow the execution of much more accurate and realistic simulations and offline programming tasks.

Despite proving to be much more efficient than the original approximation (based on two elementary rotations), the newly-created model of the mechanism is still considered as partially complete by the authors, who, based on experience, performed simulations and research, are confident that the imperfections of the GPR's components are distributed not just linearly, in a radial fashion, but practically in any direction, when tilting the platform. For this reason, the so-called enhanced virtualization approach is proposed, which, compared to the initial one, aims at providing an even more realistic description of the GPR's mobility by introducing three new virtual joints to the platform – this time rotational. Two modifications of the approach are demonstrated in the course of work, both featuring six virtual joints in total – three translational and three rotational.

IV. A GENERAL APPROACH TO VIRTUALIZATION

In order to formalize the GPR virtualization approach, let's introduce two orthonormal coordinate frames $O_b e_{b1} e_{b2} e_{b3}$ and $O_p e_{p1} e_{p2} e_{p3}$, firmly attached to the base and the platform, respectively. The centers of the spherical joints are denoted by P_k , and the intersection points of the sliding joints with the plane of the base passing through the origin O_b are denoted by B_k , $k = 1, 2, 3$. There are also multiple radius-vectors defined: $\mathbf{r}_{O_b P_k} = \overline{O_b P_k}$; $\mathbf{r}_{b k} = \overline{O_b B_k}$; $\mathbf{r}_{p k} = \overline{O_p P_k}$; $\mathbf{r}_{P_k P_l} = \overline{P_k P_l}$, see Fig. 3. The length of $\overline{B_k P_k}$ is denoted by q_k and $\mathbf{q} = (q_1 \ q_2 \ q_3)^T$ is the vector of the generalized coordinates of the manipulator.

A. Mobility and Sensitivity Analysis

The position and the orientation of all links of the GPR are uniquely defined by a set of parameters $\mathbf{P} \in \mathfrak{R}^N$, which are not

necessarily independent. A possible convenient choice for \mathbf{P} is $(\mathbf{q}^T \mathbf{r}_{O_b P_1}^T \mathbf{r}_{O_b P_2}^T \mathbf{r}_{O_b P_3}^T)^T$. The equations of constraints imposed on \mathbf{P} by the mechanism are:

$$\Phi: \mathfrak{R}^N \rightarrow \mathfrak{R}^N: \Phi(\mathbf{P}) = \mathbf{0} \quad (1)$$

Given the definition of \mathbf{P} with dimension $N=12$, (1) can be rewritten as:

$$\begin{aligned} \mathbf{r}_{bi} + q_i \mathbf{e}_{b3} - \mathbf{r}_{O_b P_i} &= 0, i=1,2,3 \\ (\mathbf{r}_{O_b P_{i\%3+1}} - \mathbf{r}_{O_b P_i})^2 - L_{i(i\%3+1)}^2 &= 0, i=1,2,3 \end{aligned}$$

where % represents the modulus operation.

The mobility of the GPR mechanism, characterized by its DOF, is $h = N - \text{rank}\left(\frac{\partial \Phi}{\partial \mathbf{P}}\right)$, see [11] for the definition of $\frac{\partial \Phi}{\partial \mathbf{P}}$. In the case of $q_1 = q_2 = q_3$, $\text{rank}\left(\frac{\partial \Phi}{\partial \mathbf{P}}\right) = 9$ and $h = 3$. In other words, the platform has instantaneous local mobility with dimension three. Even small differences in the coordinates q_1, q_2, q_3 , which are in the range of the normal deviations from the parallelism of the rods connecting the platform to the base, bring $\text{rank}\left(\frac{\partial \Phi}{\partial \mathbf{P}}\right)$ to 11. This means that the platform has a single DOF at the specific configuration, which is an apparent deficiency. The GPR is designed to work in a close vicinity of singular configurations ($q_1 = q_2 = q_3$). It has to perform two small independent rotations of the platform ($\pm 1.5^\circ$) about an axis, which lies in the plane of the platform, and a vertical translation in a larger range. Since $\text{rank}\left(\frac{\partial \Phi}{\partial \mathbf{P}}\right)$ is equal to 11 everywhere except for $q_1 = q_2 = q_3$, the constraints imposed to the platform by the spherical joints have to be relieved. In real, this happens naturally because of the imperfection of the joints and the inherent elasticity of the links, which compensates the two DOF deficiency. The virtualization of the mechanism comes to model this behavior. As seen from (1), the equations of constraints contain the three parameters $L_{12} L_{23} L_{31}$, which are constant in the ideal case of having all the components of the mechanism rigid, and in the lack of backlashes. Let us rewrite (1) as $\Phi(\mathbf{P}, \mathbf{L}) = \mathbf{0}$, where $\mathbf{L} = (L_{12} L_{23} L_{31})^T$, and assume that \mathbf{L} is made variable through the parameterization $\mathbf{L} = \mathbf{F}(\mathbf{X})$, $\mathbf{X} \in \mathfrak{R}^M$, $\mathbf{X} = \text{var}$. The first virtualization approach, presented in [11], had $\mathbf{X} = (l_1 l_2 l_3)^T$, where $l_k = \|\mathbf{r}_{pk}\|$, $k = 1,2,3$. Let us introduce the vector $\Psi = [\mathbf{P}^T \mathbf{X}^T]^T$, $\Psi \in \mathfrak{R}^{N+M}$ in order to further study the mobility of the GPR, augmented by virtual joints. The equation of constraints (1) can be written as:

$$\Phi(\Psi) = \Phi(\mathbf{P}, \mathbf{X}) = \mathbf{0} \quad (2)$$

with Jacobian matrix:

$$\frac{\partial \Phi}{\partial \Psi} = \begin{bmatrix} \frac{\partial \Phi}{\partial \mathbf{P}} & \frac{\partial \Phi}{\partial \mathbf{X}} \end{bmatrix} = \begin{bmatrix} \frac{\partial \Phi}{\partial \mathbf{P}} & \frac{\partial \Phi}{\partial \mathbf{L}} \frac{\partial \mathbf{L}}{\partial \mathbf{X}} \end{bmatrix} \in \mathfrak{R}^{12 \times (12+M)}$$

since $\frac{\partial \Phi}{\partial \mathbf{P}} \in \mathfrak{R}^{12 \times 12}$, $\frac{\partial \Phi}{\partial \mathbf{L}} \in \mathfrak{R}^{12 \times 3}$, $\frac{\partial \mathbf{L}}{\partial \mathbf{X}} \in \mathfrak{R}^{3 \times M}$, and $\frac{\partial \Phi}{\partial \mathbf{L}} \frac{\partial \mathbf{L}}{\partial \mathbf{X}} \in \mathfrak{R}^{12 \times M}$.

It's important to note that contrary to $\text{rank}\left(\frac{\partial \Phi}{\partial \mathbf{P}}\right)$, $\text{rank}\left(\frac{\partial \Phi}{\partial \Psi}\right)$ is always equal to 12, i.e. it does not depend on the "distance"

to a singular configuration. Therefore, the augmented GPR has always M DOF = $\text{dim}(\Psi) - \text{rank}\left(\frac{\partial \Phi}{\partial \Psi}\right) = 12 + M - 12 = M$. Let's differentiate (2) with respect to \mathbf{P} and \mathbf{X} , and evaluate the properties of the matrices $\frac{\partial \Phi}{\partial \mathbf{P}}$ and $\frac{\partial \Phi}{\partial \mathbf{X}}$:

$$\frac{\partial \Phi}{\partial \mathbf{P}} d\mathbf{P} + \frac{\partial \Phi}{\partial \mathbf{X}} d\mathbf{X} = \mathbf{0} \quad (3)$$

It will be shown that the eigenvalues and the singular values of $\frac{\partial \mathbf{X}}{\partial \mathbf{P}}$ can be effectively used in evaluating the sensitivity of the vector \mathbf{X} to variations of the vector \mathbf{P} . The matrix $\frac{\partial \Phi}{\partial \mathbf{X}}$ has three non-zero singular values, which vary slightly as the GPR moves. In particular, they are non-zero at singularity. Let $\frac{\partial \Phi}{\partial \mathbf{X}}^\dagger$ be the Moore-Penrose pseudo-inverse of $\frac{\partial \Phi}{\partial \mathbf{X}}$ [13]. From (3):

$$d\mathbf{X} = -\frac{\partial \Phi}{\partial \mathbf{X}}^\dagger \frac{\partial \Phi}{\partial \mathbf{P}} d\mathbf{P} = \frac{\partial \mathbf{X}}{\partial \mathbf{P}} d\mathbf{P}$$

The last equation will allow us to answer a very important question: "What are the boundaries of $\|d\mathbf{X}\|$ for a given $\|d\mathbf{P}\|$?", or in other words: "How big the virtual joints' motion would be for a given tilting of the platform?". To answer it, let us consider the eigenvalue decomposition of $\frac{\partial \mathbf{X}^T}{\partial \mathbf{P}} \frac{\partial \mathbf{X}}{\partial \mathbf{P}} = \mathbf{V} \mathbf{D} \mathbf{V}^T$, where $\mathbf{V} \in \mathfrak{R}^{12 \times 12}$ and its columns are the eigenvectors of $\frac{\partial \mathbf{X}^T}{\partial \mathbf{P}} \frac{\partial \mathbf{X}}{\partial \mathbf{P}}$ i.e. $\mathbf{V} = (\mathbf{v}_1, \mathbf{v}_2, \dots, \mathbf{v}_{12})$, and $\mathbf{D} = \text{diag}(d_1, d_2, \dots, d_{12})$ is a diagonal matrix, containing the eigenvalues of $\frac{\partial \mathbf{X}^T}{\partial \mathbf{P}} \frac{\partial \mathbf{X}}{\partial \mathbf{P}}$, arranged in an ascending order, i.e. $d_1 < d_2 < \dots < d_{12}$ [14]. Since $\text{rank}\left(\frac{\partial \mathbf{X}}{\partial \mathbf{P}}\right)$ is equal to three, only d_{10}, d_{11} and d_{12} are nonzero, and it becomes obvious that:

$$0 \leq \|d\mathbf{X}\|^2 = d\mathbf{P}^T \frac{\partial \mathbf{X}^T}{\partial \mathbf{P}} \frac{\partial \mathbf{X}}{\partial \mathbf{P}} d\mathbf{P} \leq d_{12} \|d\mathbf{P}\|^2$$

However, the last inequality is not strong enough and we would like to derive another inequality, which defines closer boundaries of $\|d\mathbf{X}\|$ by taking into consideration the fact that only three eigenvalues of $\frac{\partial \mathbf{X}^T}{\partial \mathbf{P}} \frac{\partial \mathbf{X}}{\partial \mathbf{P}}$ are nonzero, namely:

$$\sqrt{d_{10} \sum_{k=10}^{12} (\mathbf{v}_k^T d\mathbf{P})^2} \leq \|d\mathbf{X}\| \leq \sqrt{d_{12} \sum_{k=10}^{12} (\mathbf{v}_k^T d\mathbf{P})^2} \quad (4)$$

$$\sigma^{\min} \left(\frac{\partial \mathbf{X}}{\partial \mathbf{P}} \right) \sqrt{\sum_{k=10}^{12} (\mathbf{v}_k^T d\mathbf{P})^2} \leq \|d\mathbf{X}\| \leq \sigma^{\max} \left(\frac{\partial \mathbf{X}}{\partial \mathbf{P}} \right) \sqrt{\sum_{k=10}^{12} (\mathbf{v}_k^T d\mathbf{P})^2} \quad (5)$$

where $\sigma^{\min} \left(\frac{\partial \mathbf{X}}{\partial \mathbf{P}} \right)$ is the minimum nonzero and $\sigma^{\max} \left(\frac{\partial \mathbf{X}}{\partial \mathbf{P}} \right)$ is the maximum singular values of $\frac{\partial \mathbf{X}}{\partial \mathbf{P}}$. Inequalities (4) and (5) define the lower and the upper bounds of $\|d\mathbf{X}\|$ for a given $\|d\mathbf{P}\|$.

B. Kinematic Transformations Between \mathbf{X} and \mathbf{L}

The relationship between vectors \mathbf{X} and \mathbf{L} is of significant importance for the solution of the direct and inverse kinematic problems of the augmented GPR mechanism. Normally, the vectors \mathbf{X} and \mathbf{L} are implicitly related through the equation:

$$\mathbf{F}(\mathbf{X}, \mathbf{L}) = \mathbf{0} \quad (6)$$

The explicit solution of (6) for \mathbf{X} in both virtualization cases of this study is quite difficult and that's why (6) is solved for

\mathbf{X} by using the well-known Newton-Raphson iterative method. The last requires knowledge of the matrix $\frac{\partial \mathbf{X}}{\partial \mathbf{L}}$ and the solution for \mathbf{X} is $\mathbf{X}_k = \mathbf{X}_{k-1} + \frac{\partial \mathbf{X}}{\partial \mathbf{L}}(\mathbf{L} - \mathbf{L}_{k-1})$, $k=1, 2, \dots$. Normally it takes 2–3 iterations to find a very accurate solution if the initial value of \mathbf{X} corresponds to $q_1 = q_2 = q_3$.

V. EXTENDED VIRTUALIZATION OF THE GPR

A. Augmented Vector \mathbf{X} , Described in Terms of l and φ

Considering the general virtualization approach, introduced above, the geometry of the GPR mechanism can be represented by the following parameters: $\mathbf{X} = (l_1 \ l_2 \ l_3 \ \varphi_1 \ \varphi_2 \ \varphi_3)^T$ and $\mathbf{L} = (L_{12} \ L_{23} \ L_{31})^T$, as shown in Fig. 4 (left). In this case, (6) becomes:

$$l_i^2 + l_{i\%3+1}^2 - 2l_i l_{i\%3+1} \cos(120^\circ - \varphi_i + \varphi_{i\%3+1}) - L_{i(i\%3+1)}^2 = 0, \quad i = 1, 2, 3$$

The matrices $\frac{\partial \mathbf{F}}{\partial \mathbf{X}} \in \mathfrak{R}^{3 \times 6}$ and $\frac{\partial \mathbf{F}}{\partial \mathbf{L}} \in \mathfrak{R}^{3 \times 3}$ can be represented as:

$$\frac{\partial \mathbf{F}}{\partial \mathbf{X}} = \begin{pmatrix} 2l_1 - 2l_2 c(120^\circ - \varphi_1 + \varphi_2) & 0 & 2l_3 - 2l_1 c(120^\circ - \varphi_3 + \varphi_1) \\ 2l_2 - 2l_1 c(120^\circ - \varphi_1 + \varphi_2) & 2l_2 - 2l_3 c(120^\circ - \varphi_2 + \varphi_3) & 0 \\ 0 & 2l_3 - 2l_2 c(120^\circ - \varphi_2 + \varphi_3) & 2l_1 - 2l_3 c(120^\circ - \varphi_3 + \varphi_1) \\ -2l_1 l_2 s(120^\circ - \varphi_1 + \varphi_2) & 0 & -2l_3 l_1 s(120^\circ - \varphi_3 + \varphi_1) \\ 2l_1 l_2 s(120^\circ - \varphi_1 + \varphi_2) & -2l_2 l_3 s(120^\circ - \varphi_2 + \varphi_3) & 0 \\ 0 & 2l_2 l_3 s(120^\circ - \varphi_2 + \varphi_3) & 2l_3 l_1 s(120^\circ - \varphi_3 + \varphi_1) \end{pmatrix}^T$$

where $s(\cdot)$ denotes $\sin(\cdot)$ and $c(\cdot)$ denotes $\cos(\cdot)$.

$$\frac{\partial \mathbf{F}}{\partial \mathbf{L}} = \text{diag}(-2L_{12}, -2L_{23}, -2L_{31}) \quad (7)$$

The matrix $\frac{\partial \mathbf{X}}{\partial \mathbf{L}}$ needed to solve (6) for \mathbf{X} is:

$$\frac{\partial \mathbf{X}}{\partial \mathbf{L}} = -\left(\frac{\partial \mathbf{F}}{\partial \mathbf{X}}\right)^\dagger \frac{\partial \mathbf{F}}{\partial \mathbf{L}} = -\frac{\partial \mathbf{F}^T}{\partial \mathbf{X}} \left(\frac{\partial \mathbf{F}}{\partial \mathbf{X}} \frac{\partial \mathbf{F}^T}{\partial \mathbf{X}}\right)^{-1} \frac{\partial \mathbf{F}}{\partial \mathbf{L}} \quad (8)$$

B. Augmented Vector \mathbf{X} , Described in Terms of dr and $d\varphi$

Another possible way of describing the mobility of the GPR by using the same concept of three translational and three revolute virtual joints is associated with the introduction of an augmented vector \mathbf{X} , described in terms of coordinates dr and $d\varphi$, as shown in Fig. 4 (right). In contrast to the previous method, where the effect of backlash and elasticity is represented as a portion of a disc, the newly introduced augmented vector \mathbf{X} represents the more realistic scenario where the imperfections of the GPR are evenly distributed, taking the shape of a circle.

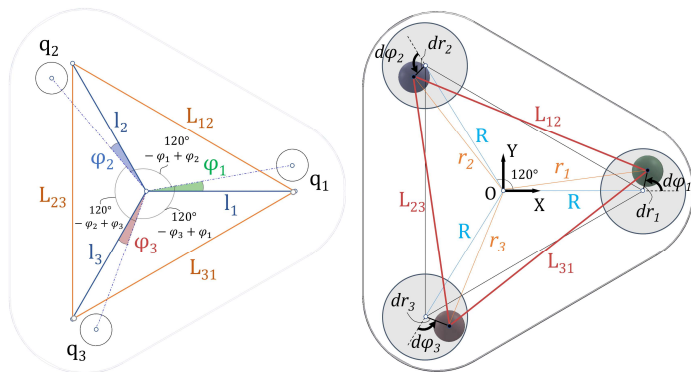


Figure 4. Visualization of the virtual joints of the two extended GPR models.

Considering the modeling modification, described in terms of dr and $d\varphi$ coordinates, the geometry of the GPR can be represented by the following equations:

$$(\mathbf{r}_{i\%3+1} - \mathbf{r}_i)^T (\mathbf{r}_{i\%3+1} - \mathbf{r}_i) - L_{i(i\%3+1)}^2 = 0, \quad i=1, 2, 3, \text{ where}$$

$$\begin{aligned} \mathbf{r}_1 &= [R + dr_1 \cos(d\varphi_1) \quad dr_1 \sin(d\varphi_1)]^T \\ \mathbf{r}_2 &= [R \cos(120^\circ) + dr_2 \cos(120^\circ + d\varphi_2) \quad R \sin(120^\circ) + dr_2 \sin(120^\circ + d\varphi_2)]^T \\ \mathbf{r}_3 &= [R \cos(240^\circ) + dr_3 \cos(240^\circ + d\varphi_2) \quad R \sin(240^\circ) + dr_3 \sin(240^\circ + d\varphi_3)]^T \end{aligned}$$

The matrix $\frac{\partial \mathbf{F}}{\partial \mathbf{X}} \in \mathfrak{R}^{3 \times 6}$ can be represented as:

$$\frac{\partial \mathbf{F}}{\partial \mathbf{X}} = \begin{pmatrix} 2(\mathbf{r}_2 - \mathbf{r}_1)^T \partial(\mathbf{r}_2 - \mathbf{r}_1) / \partial X_1 & 0 & 2(\mathbf{r}_1 - \mathbf{r}_3)^T \partial(\mathbf{r}_1 - \mathbf{r}_3) / \partial X_1 \\ 2(\mathbf{r}_2 - \mathbf{r}_1)^T \partial(\mathbf{r}_2 - \mathbf{r}_1) / \partial X_2 & 2(\mathbf{r}_3 - \mathbf{r}_2)^T \partial(\mathbf{r}_3 - \mathbf{r}_2) / \partial X_2 & 0 \\ 0 & 2(\mathbf{r}_3 - \mathbf{r}_2)^T \partial(\mathbf{r}_3 - \mathbf{r}_2) / \partial X_3 & 2(\mathbf{r}_1 - \mathbf{r}_3)^T \partial(\mathbf{r}_1 - \mathbf{r}_3) / \partial X_3 \\ 2(\mathbf{r}_2 - \mathbf{r}_1)^T \partial(\mathbf{r}_2 - \mathbf{r}_1) / \partial X_4 & 0 & 2(\mathbf{r}_1 - \mathbf{r}_3)^T \partial(\mathbf{r}_1 - \mathbf{r}_3) / \partial X_4 \\ 2(\mathbf{r}_2 - \mathbf{r}_1)^T \partial(\mathbf{r}_2 - \mathbf{r}_1) / \partial X_5 & 2(\mathbf{r}_3 - \mathbf{r}_2)^T \partial(\mathbf{r}_3 - \mathbf{r}_2) / \partial X_5 & 0 \\ 0 & 2(\mathbf{r}_3 - \mathbf{r}_2)^T \partial(\mathbf{r}_3 - \mathbf{r}_2) / \partial X_6 & 2(\mathbf{r}_1 - \mathbf{r}_3)^T \partial(\mathbf{r}_1 - \mathbf{r}_3) / \partial X_6 \end{pmatrix}^T$$

The matrices $\frac{\partial \mathbf{F}}{\partial \mathbf{L}}$ and $\frac{\partial \mathbf{X}}{\partial \mathbf{L}}$ are given by (7) and (8), respectively.

VI. SIMULATIONS

The main focus of the simulation study is to experimentally evaluate the relationship between the motion of the virtual joints and the motion of the platform, with emphasis on the singular configurations, which are considered as working configurations. The GPR mechanism was given a cyclic motion, varying the generalized coordinates (q_1, q_2, q_3) in such a way that the platform repeatedly passes through singularity.

A. Simulation of the Extended GPR Model (l and φ)

Subject of the first simulation study is the extended GPR model containing six virtual joints, described in terms of l and φ coordinates. The goal is to derive the relationship between the motion of the platform $\mathbf{X} = (l_1 \ l_2 \ l_3 \ \varphi_1 \ \varphi_2 \ \varphi_3)^T$ and $\mathbf{L} = (L_{12} \ L_{23} \ L_{31})^T$. The simulation process is a sequence of moves (samples), corresponding to *yaw* and *pitch* rotations of the platform, defined by γ and α angles, respectively. For each $\gamma [0^\circ \div 360^\circ]$ the α changes in the interval $[-2^\circ \div 2^\circ]$ by a step of 0.2° . A number of zoomed-in graphs represent the behavior of the GPR in a vicinity of singular configurations, $q_1 = q_2 = q_3 = 500$ mm (Fig. 5). At singularity, l_1, l_2, l_3 reach their extremum $l_1 = l_2 = l_3 = 93.218$ (Fig. 6). In other words, the platform performs rotation at the expense of minimal linear motion of l_1, l_2 and l_3 . Similarly, the angular components of \mathbf{X} (φ_1, φ_2 and φ_3), shown in Fig. 7, and the components of the vector \mathbf{L} (L_{12}, L_{23} and L_{31}), shown in Fig. 8, reach their extremum at singular configurations. It is obvious from Fig. 7 that the deviation of φ_1, φ_2 and φ_3 is negligibly small – a fact that confirms the validity of the initial virtualization approach, based on three sliding joints.

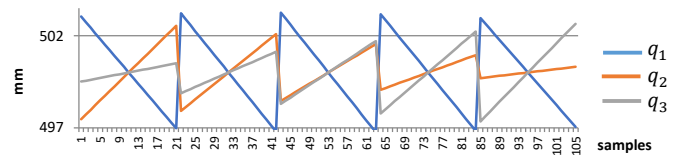


Figure 5. Zoomed-in of the GPR generalized coordinates displacements.

VII. CONCLUSION

The presented work contributes to the process of modeling, studying and simulating the mobility and accuracy of the GPR manipulator by introducing an original concept for robot joint virtualization. Based on this approach, two extended kinematic models of the overconstrained mechanism, both featuring six virtual joints (three translational and three revolute), have been developed. The last are exhaustively studied by using methods from the analytical mechanics in order to find the relationship between the finite rotations of the platform and the inherent imperfections of the GPR components, responsible for the three-degree-of-freedom mobility of the actual manipulator. The Eigen Decomposition of the Jacobian matrices of the equations of constraints imposed on the platform was found to be an efficient tool for determining the boundaries of the virtual joints' motion (which was proved to be very small and within the range of the inherent imperfections), required for the execution of a specific tiling of the platform when near singular configurations. The introduction of three additional (revolute) virtual joints results in the development of precise computational models that provide a realistic representation of the GPR's overconstrained behavior, allowing their further use with the already implemented SolidWorks API-based tool for motion simulation and offline programming purposes essential for the industrial application of the GPR mechanism.

REFERENCES

- [1] Ö. Selvi, "Structural and kinematic synthesis of overconstrained mechanisms," Ph.D. thesis, Izmir, 2012.
- [2] G. Gogu, "Structural and Kinematic Analysis and Synthesis of Parallel Robots," SSIR-Clermont-Ferrand, June 27, 2008.
- [3] S. Guo, H. Qu, Y. Fang, C. Wang, "The DOF Degeneration Characteristics of Closed-Loop Overconstrained Mechanisms," Transactions of the Canadian Society for Mechanical Engineering, vol. 36, no. 1, 2012.
- [4] Z. Sotirov, "Parallel-Serial Manipulators in Semiconductor Automation," Semiconductor European, July 2002.
- [5] O. Hamdoun, L. Bakkali, F. Baghli, "Analysis and Optimum Kinematic Design of a Parallel Robot," 10th International Conference Interdisciplinarity in Engineering, INTER-ENG 2016.
- [6] A. Pashkevich, D. Chablat, P. Wenger, "Stiffness Analysis of Overconstrained Parallel Manipulators," Mechanism and Machine Theory, 44(5), pp. 966–982, May 2009.
- [7] A. Hovenaars, P. Lambert, J. Herder, "Jacobian-based stiffness analysis method for parallel manipulators with non-redundant legs," Journal of Mechanical Engineering Science, vol. 230(3), pp. 341–352, 2016.
- [8] Y. Patel, P. George, "Parallel Manipulators Applications – A Survey," Modern Mechanical Engineering 2(03), pp. 57–64, August 2012.
- [9] G. Genov, D. Todorov, "Universally Tilttable Z-Axis Drive," U.S. Patent US5954840, June 13, 1996.
- [10] G. Genov, Z. Sotirov, E. Bonev, "Robot Motion Compensation System," U.S. Patent US6489741B1, August 1998.
- [11] N. Bratovanov, Z. Sotirov, V. Zamanov, "Modeling and Simulation of Overconstrained Closed-Loop Mechanisms," Proceedings of Technical University of Sofia, vol. 67, no. 2, pp. 81–90, 2017.
- [12] N. Bratovanov, "Robot Modeling, Motion Simulation and Off-line Programming Based on SolidWorks API," Third IEEE International Conference on Robotic Computing (IRC), vol.1, pp. 574–579, 2019.
- [13] A. Ben-Israel, T.N.E. Greville, "Generalized Inverses: Theory and Applications (2nd Edition)," Springer-Verlag, New York, 2003.
- [14] L. Hogben, K. Rosen, "Handbook of Linear Algebra," Taylor & Francis Group, 2007.

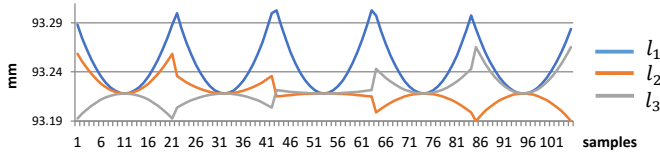


Figure 6. Zoomed-in of vector \mathbf{X} linear components displacements.

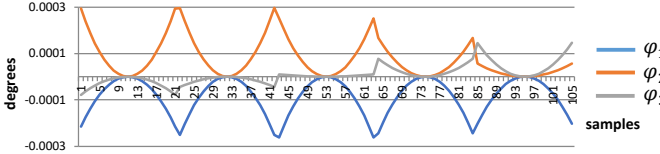


Figure 7. Zoomed-in of vector \mathbf{X} angular components displacements.

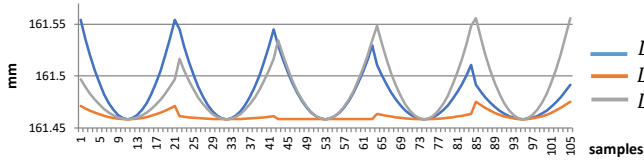


Figure 8. Zoomed-in of vector \mathbf{L} components displacements.

B. Simulation of the Extended GPR Model (dr and $d\varphi$)

The second simulation study is similar and is dedicated to the extended GPR model with six virtual joints, described in terms of dr and $d\varphi$ coordinates. As with the first simulation study, the goal is to define the relationship between the tilt of the platform, the parameters describing the virtual joints $\mathbf{X} = (dr_1 \ dr_2 \ dr_3 \ d\varphi_1 \ d\varphi_2 \ d\varphi_3)^T$ and the vector \mathbf{L} . The analysis is based on the identical motion of the platform, already introduced in the previous study. The linear (dr) and the angular ($d\varphi$) components of vector \mathbf{X} are shown in Fig. 9 and Fig. 10. Fig. 11 plots the variations of the components of \mathbf{L} . The graphs indicate that the angular displacements of the virtual joints (corresponding to the imperfections of the real spherical bearing in the direction, perpendicular to their radial axes) are negligibly small.

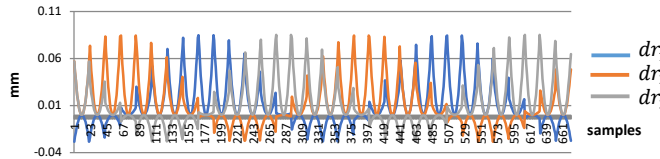


Figure 9. Displacements of the linear components of vector \mathbf{X} .

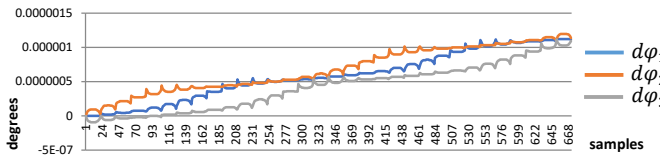


Figure 10. Displacements of the angular components of vector \mathbf{X} .

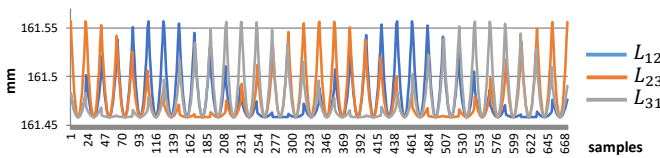


Figure 11. Displacement of the components (linear) of vector \mathbf{L} .